Measurement of dynamic/advancing/receding contact angle by video-enhanced sessile drop tensiometry

Shi-Yow Lin,[a] Hong-Chi Chang, Lung-Wei Lin, and Pao-Yao Huang
Department of Chemical Engineering, National Taiwan Institute of Technology, Taipei, 106, Taiwan, Republic of China

(Received 8 April 1996; accepted for publication 8 May 1996)

A sessile drop tensiometer enhanced by video-image digitization is designed for the experimental measurement of dynamic/advancing/receding contact angle. A collimated light beam passes through the sessile drop of liquid and a silhouette of the drop is created. The equipment video images the silhouette, digitizes the image, and locates the edge coordinates of the drop. A new technique, replacing the classical selected plane method, is developed to obtain the values of capillary constant and the radius of curvature at apex from the edge coordinates of digitized drop profile. Four parameters (location of apex, radius of curvature at apex, and the capillary constant) are calculated from the best fit between the edge coordinates and the theoretical curve obtained from the Laplace equation. The contact angle is then obtained from the location of the air/solid interface and the best-fitted sessile drop profile. By controlling the humidity of air phase surrounding the drop, this technique can measure the advancing and receding contact angles and monitor the rate of advancing and receding of the three-phase line simultaneously. This technique works well on contact angle measurement for sessile drops with or without an equator. Preliminary studies on the dynamic contact angle have been made for water drops on paraffin, polymethylmethecrylate, and glass. The technique is capable of giving contact angle of 0.2° precision. © *1996 American Institute of Physics.* [S0034-6748(96)04208-6]

INTRODUCTION

Sessile drop tensiometry, enhanced by video-image digitization, is one of the most popular techniques for measuring the contact angle of fluid/fluid/solid or fluid/fluid/fluid interfaces now. This technique is capable for static and dynamic contact angles and applicable to large and small angle measurements. Experimentally, it needs only small amounts of liquid and requires only a few square millimeters of substrate.

There are several techniques available for measuring the contact angle θ.[1] The most commonly used method is that measuring θ directly for a drop of liquid resting on a flat solid surface by placing a tangent at the contact point of the gas/liquid/solid interface. If a spherical shape is assumed, the contact angle may be obtained using the so called $\theta/2$ method,[2] in which only the height of the sessile drop and the diameter of the three-phase line are needed. Fitting three or five interfacial loci with a polynomial equation is also another convenient way to get the contact angle.[3] The Wilhelmy slide technique[4] and the video-enhanced plate method[5] are suitable for the study of dynamic behavior of contact angle. Regarding the methods applicable to advancing and receding contact angle, there are the captive bubble method,[1] the dynamic contact angle analysis technique,[6] the sessile drop on a tilting plate method,[7] and the tilting plate technique.[8]

The direct technique is the most obvious way of determining the contact angles from sessile drops. The accuracy of this technique is claimed to be $\pm 2°$. The major drawbacks of the direct technique are

(i) the difficulty of locating the contact point precisely from the photograph or image;
(ii) lack of information for identifying the angle measured being advancing, equilibrium, receding, or neither of them.

Skinner, Rotenberg, and Neumann[9] and Mooy *et al.*[10] developed an axisymmetric drop shape analysis for measuring contact angle. This method needs no information about the contact point, but more information (such as surface tension, drop volume, and equatorial diameter or the diameter of three-phase contact circle) is needed. Estimation of surface tension and contact angle from the sessile drop shapes was also proposed by Huh and Reed[11] and Rotenberg, Boruvka, and Neumann.[12] This method avoids the first drawback stated above, but no information regarding the second one is given. One more drawback for the method using the drop shapes in Refs. 11 and 12 is that only the drop with an equator can be measured.

In this work a video-enhanced sessile drop tensiometer was developed to measure the dynamic contact angle. From the relaxation of contact angle, the advancing and receding contact angles are identified. The surface tension is also obtained but may be not very precisely if the contact angle of the sessile drop is small. Traditionally, the sessile drop method uses a selected plane technique[11] that requires only the equatorial diameter d_e and the distance Z_e from the plane with the equator to the apex to determined the surface tension. The accuracy of this method is improved greatly with video-image digitization. By this means, the interface loci of the drop are found and fitted with a theoretical interface profile generated from the Laplace equation. The regression result therefore yields the optimum surface tension and contact

[a]Author to whom correspondence should be addressed.

 0034-6748/96/67(8)/2852/7/$10.00

angle. The success of the regression relies on a set of initial values of parameter for the numerical method (e.g., fourth-order Runge–Kutta method), to find out the optimum congruence between the experimental data and theoretical profiles. These parameters include the location of apex X_0, Z_0, radius of curvature at apex R_0, and the capillary constant $B = \Delta\rho g R_0^2/\gamma$ (γ is surface tension). The values of B and R_0 from the classical selected plane technique with d_e and Z_e of sessile drop method are usually used as the initial guess of the numerical calculation if the liquid drop has an equator. Unfortunately, for the drop with contact angle which is around or less than 90°, using the drop profile to obtain the more accurate contact angle is still not available.

The aim of this article is to use the video-enhanced sessile drop tensiometry to measure the dynamic/advancing/receding contact angle for both types of sessile drops which have an equator ($\theta > 90°$) or have no equator ($\theta < 90°$). A new technique is developed to obtain the initial values of B and R_0 when the sessile drops have no equator, and it also works for drops having an equator. The idea comes from the modified pendant drop method for the low interfacial tension measurement.[13] In this method, two interfacial loci (P_1 and P_2 on the profile of drop in Fig. 3) are selected to replace the roles of d_e (equatorial diameter) and Z_e (the distance from the plane with the equator to the apex) in the classical technique. Note that the values of B and R_0 obtained from this technique are more accurate if interfacial loci closer to the fluid–fluid–solid three-phase line are selected. This is because the drop profiles of two different values of capillary constant B (see Fig. 4 for $R_0 = 1$) depart further from each other at interfacial loci further from the apex. A function of drop shape X_i ($i = A_1$ or A_2) is defined as the value of X_j/R_0 of interfacial locus P_j ($j = 1$ or 2) in which $X_j/Z_j = i$. The selected points P_1 (with drop shape function X_{A_1}) and P_2 (with drop shape function X_{A_2}) are unique at a specific value of capillary constant. The details of X_i and how P_1 and P_2 are elected are described later.

The unique features of the present method are:

(i) It can measure advancing and receding contact angles (to 0.2° precision) and surface tension simultaneously;
(ii) a new technique is developed to evaluate B and R_0 to improve the measurement of contact angle from the sessile drop profile for drops having no equator; and
(iii) it can monitor the rate of advancing and receding of the three-phase line.

These unique features make it useful in the study of dynamic behavior of liquid drops on a flat solid surface. It also has the potential usage to measurements of contact angle and surface tension for drops of surfactant solutions spreading on a flat solid surface.

CONSTRUCTION PRINCIPLES

A schematic diagram of the video-image enhanced sessile drop tensiometer is given in Fig. 1. The equipment is used to create a silhouette of a sessile drop, to video image the silhouette, and to digitize the image. The equipment consists of an image forming and recording system, a drop forming system, an air thermostat and humidity system, and a video-image profile digitizer.

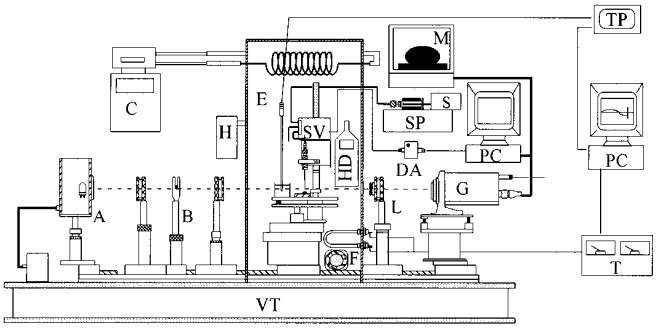

FIG. 1. Schematic of sessile drop tensiometry apparatus and the video digitization equipment. A: light source; B: pin hole, filter, and plano-convex lens; C: circulator; DA: D/A data translation card; B: thermostatic air chamber; F: fan; G: video camera; H: humidifier; HD: humidity detector; L: objective lens; M: monitor; PC: personal computer; S: syringe; SP: syringe pump; SV: solenoid valve; T: heater; TP: thermistor probe; VT: vibration-less table.

The image forming and recording system consists of a light source (a halogen lamp with constant light intensity; Oriel, QTH No. 63200), a lens system for producing a collimated beam, an objective lens (effective focal length 60 mm, f/no. 7.1), a video recorder (VO-9600, Sony) with frame code generator (FCG-700, Sony), and a solid-state video camera (MS-4030 CCD, Sierra, Scientific Co.) The lens system consists of a plano-convex lens, a quartz ND filter, and a pinhole. All these parts are installed on adjustable stages (with freedom of XYZ, rotation, and tilting) which are placed on a vibration isolated workstation.

The drop forming system consists of a stainless-steel needle which is connected to the normally closed port of a three-way miniature solenoid valve (Lee Co.) via 1/16 in. i.d. Teflon tubing. The common port of the valve is connected to a gas-tight Hamilton syringe placed in a syringe pump (Sage Instruments). The valve is controlled by the output signal of a D/A data translation card (DT 2801) installed on a personal computer. The video-image digitizer (DT 2861 Arithmetic Frame Grabber, Data Translation), also installed on the computer, digitizes the picture into 480 lines$\times$512 pixels and assigns to each one a level of gray with 8 bit resolution. The maximum rate with which an image can be digitized is 1/30 s.

The air thermostat and humidity system comprises an air chamber, an air fan, a heater, a cooling coiled copper pipe, a thermistor probe, a humidifier, and a humidity detector. The humidifier and humidity detector are connected to the air chamber to increase and to monitor the humidity of the air inside the chamber. The air chamber is made of 1-cm-thick polymethylmethacrylate (PMMA) and the coiled copper pipe is connected to a refrigerated circulator outside the air chamber. A personal computer collects the temperature from the thermistor probe via a thermometer and controls a power supplier (with a PID control[18]) which is connected with the heat generator. The temperature stability of the air thermostat is better than ± 0.1 K.

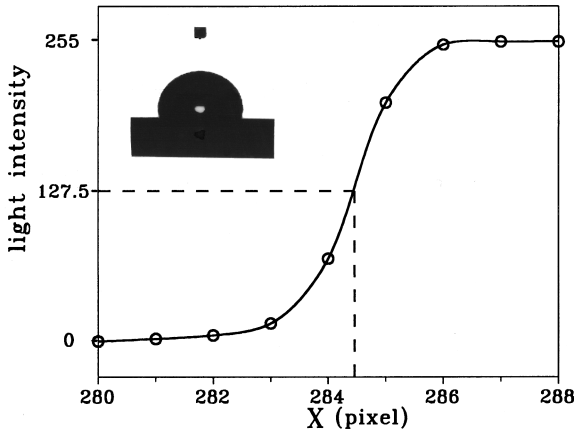

FIG. 2. Sample digitized image of water drop on PMMA solid surface and the edge location determination from digitized image profile.

IMAGE ACQUISITION AND DATA PROCESSING

An edge detection routine is devised to locate the interface contour from the digitized image, and a calibration procedure using stainless-steel balls (1.577 ± 0.002 mm and 1.983 ± 0.002 mm, calibrated by a digital linear gauge, PDN-12N, Ozaki Mfg. Co.) is applied to determine the length between pixels along a row and along a column. The calibration procedure yields values of 100.86 pixels/mm horizontally and 124.56 pixels/mm vertically.

Figure 2 is an example of the original image of a sessile liquid drop. According to the digitized image, the gray level changes from the dark inside (0 level) to the bright outside (255 level) in a few pixels, as shown in Fig. 2. This change is continuous and symmetric around 127.5, and therefore the edge is defined as the x or z position for the interpolated line corresponding to intensity 127.5. The location procedure is performed in the coordinate direction, in which the normal to the surface has the larger component.[14] Thus, near the apex the edge location is done along the z direction, while near the sides of the drop it is done along the x direction.

The experimental protocol was as follows: The solid object was initially placed on the stage in the air thermostat and was leveled by adjusting the stage. The humidity in chamber was increased by the humidifier and was kept around 95%. The water drop was then created on the solid surface using the drop forming system. The moment of drop created is set as $t=0$. Sequential digital images were then taken of the drop, first at intervals of approximately 0.1 s and then later in intervals of the order of seconds. At $t=60$ s, the humidifier was turned off and the door of the air chamber was open. The humidity outside the chamber was about 65%. The humidity around the water drop was then decreases from 95 to 65 in about 20 min. All experiments were undertaken at 25.0 ± 0.1 °C. After the contact angle relaxation was complete the images were processed to determined the drop edge coordinates.

CONTACT ANGLE CALCULATED FROM THE DROP PROFILE

The theoretical shape of the sessile drop is derived from the classical Laplace equation that relates the pressure difference across a curved interface,

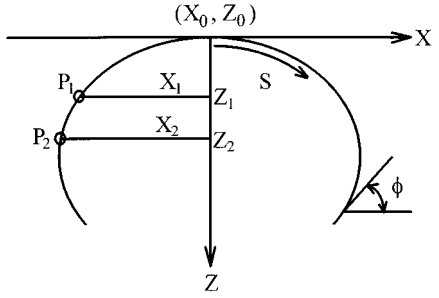

FIG. 3. Coordinate system of sessile drop and two selected interfacial loci P_1, P_2.

$$\gamma\left(\frac{1}{R_1}+\frac{1}{R_2}\right)=\Delta P, \tag{1}$$

where γ is the interfacial tension, R_1 and R_2 are the two principal radii of curvature of the interface, and ΔP is the pressure difference across the interface. For the sessile drop geometry, Eq. (1) can be recast as a set of three first-order differential equations for the spatial positions x and z and turning angle ϕ of the interface as a function of the arc length s (see Fig. 3). Using the dimensionless variables $x'=x/R_0$, $z'=z/R_0$, and $s'=s/R_0$, the first-order equations have the following form:[12]

$$\begin{aligned}\frac{d\phi}{ds'}&=2+Bz'-\frac{\sin\phi}{x'},\\ \frac{dx'}{ds'}&=\cos\phi,\\ \frac{dz'}{ds'}&=\sin\phi,\end{aligned} \tag{2}$$

where B is the capillary constant and is defined by $(\Delta\rho g R_0^2/\gamma)$, and $\Delta\rho$ is the density difference between the fluid phases and g is the gravitational acceleration constant. The equations are subject to the boundary conditions $x'(0)=z'(0)=\phi(0)=0$. Equation (2) was integrated by using a fourth-order Runge–Kutta scheme[15] initialized with an approximate solution,[11]

$$\begin{aligned}x'&=s',\\ z'&=\frac{2}{-B}\left[1-I_0(\sqrt{B}x')\right],\\ \phi&=\frac{2}{\sqrt{B}}I_1(\sqrt{B}x'),\end{aligned} \tag{3}$$

which is valid near the apex where $\phi \ll 1$. Here $I_n(x')$ is the modified Bessel function of the first kind.

The contact angle is computed from the data of drop edge coordinates and the theoretical curve in the following way. An objective function is defined as the sum of squares of the normal distance d_n between the measured points u_n and the calculated curve v obtained from the integration of Eq. (2) (i.e., $E=\Sigma_{n=1}^{N}[d_n(u_n,v)]^2$; N is the total number of experimental points). The objective function depends on four unknown variables: the actual location of the apex (X_0 and

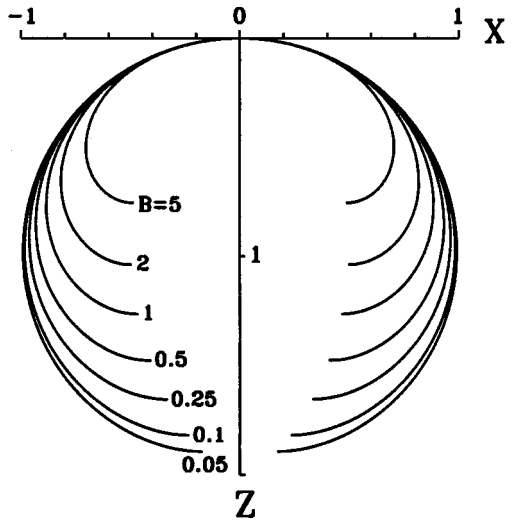

FIG. 4. Sessile drop profiles calculated from Eq. (2) for different values of capillary constant $R_0=1$.

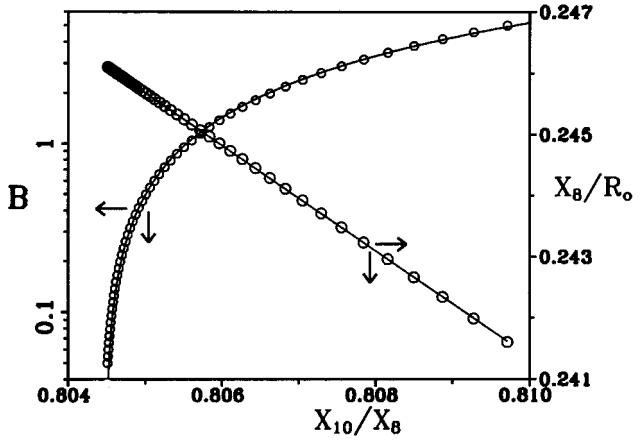

FIG. 5. Representative relationships of (a) capillary constant B vs X_{A_1}/X_{A_2} and (b) X_{A_2}/R_0 vs X_{A_1}/X_{A_2}. $A_1=10$ and $A_2=8$.

Z_0), the radius of curvature at the apex R_0, and the capillary constant B. To obtain the optimum congruence between the theoretical curve and the data points, the objective function is minimized with respect to the four parameters ($\partial E/\partial q_i=0$, $i=1-4$). Minimization equations are solved by applying directly the Newton–Raphson method.[15] The contact angle θ and surface tension γ can then be computed from the optimum values of R_0 and B and the position of the air–solid interface (see also Fig. 4). The contact angle θ is set to be $\phi\pm\theta_s$, where ϕ is the turning angle of the intercept point between the theoretical sessile drop profile and air–solid interface and θ_s is the tiny tilting angle of the solid interface from the level. θ_s is usually less than 0.2°.

From the data set there are approximately 200–600 (depending on the drop volume) measured coordinates of the drop edge for each image of drop of different volume. To obtain d_n for each point, first a theoretical curve consisting of 7000 points is generated, and then d_n is computed as the distance from the experimental point to the closest of the discrete theoretical points. Initial guesses for the Newton–Raphson procedure are obtained in the following way: X_0 is initially guessed as the centroid of the 200–600x location data points, and Z_0 as the average of the three highest z coordinates. Initial guesses for R_0 and B are obtained as follows.

(i) If the contact angle of the sessile drop is much larger than 90°, the drop has a clear equator. X_e, the radius of the circle with the maximum diameter, and Z_e, the distance between the plane with X_e and the apex, are used widely for finding B. The values of X_e and Z_e are obtained from the raw data. By integrating Eq. (2) for different values of B, graphs can be constructed of B as a function of X_e/Z_e and X_e/R_0 as a function of X_e/Z_e. The best fit of the curves can be described by polynomial equations that are summarized in Table I. The values of X_e and Z_e were obtained from the raw data, S, B, R_0, and therefore γ and θ were then calculated from Eqs. (4) and (5) and the best-fit program. Two to five iterations are necessary for the program to converge, and the standard deviation of the distance between a measured point and the calculated curve is about 0.1 pixel (≈ 1 μm).

(ii) If the drop has no clear equator (the contact angle is around or less than 90°), the technique described above does not work again. A new method is developed to obtain an accurate initial guess for B and R_0 as follows: Two interfacial loci, $P_1=(X_1,Z_1)$ and $P_2=(X_2,Z_2)$, on the profile of drop are selected from the raw data to replace the roles of Z_e and X_e. Here, X_1,X_2 and Z_1,Z_2 are the distances of the loci P_1,P_2 away from the apex of the drop in x and z directions, respectively. Define a function of drop shape X_{A_1} as the value of X_1/R_0 of the interfacial locus P_1 in where the ratio of X_1/R_0 and Z_1/R_0 is equal to A_1 (i.e., $X_1/Z_1=A_1$). Similarly, X_{A_2} is the value X_2/R_0 of point P_2 in where $X_2/Z_2=A_2$. By integrating Eq. (2) for different values of B, graphs can be constructed of B as a function of X_{A_1}/X_{A_2}, and X_{A_2}/R_0 as a function of X_{A_1}/X_{A_2}. Two typical curves are shown in Fig. 5 and the best fits of the curves can be described by polynomial equations that are summarized in Table II. As the values of A_1,A_2 are selected, P_1, P_2, X_1, X_2, Z_1, and Z_2 are known from the raw data, and therefore B and R_0 can be obtained. Three to seven iterations are necessary for the program to converge, and the standard deviation of the distance between a measured point and the calculated

TABLE I. Constants of polynomial equation relating B and X_e/Z_e and relating X_e/R_0 and X_e/Z_e ($0.1<B<100$). $B=a_0+a_1x+a_2x^2+a_3x^3$, $X_e/R_0=b_0+b_1x+b_2x^2$ ($x=X_e/Z_e$).

B	X_e/Z_e	a_0	a_1	a_2	a_3	b_0	b_1	b_2
0.1–1	1.0220–1.1547	11.8176	−7.5811	15.7715	0	1.746 57	−0.745 844	0
1–10	1.1547–1.5566	−60.3507	156.189	−140.851	44.6799	2.033 17	−1.216 35	0.193 03
10–100	1.5566–2.1837	−856.327	1574.7	−985.77	212.99	2.055 81	−1.264 35	0.214 365

TABLE II. Constants of polynomial equation relating B and X_{A_1}/X_{A_2} and relating X_{A_1}/R_0 and X_{A_1}/X_{A_2} $(0.05<B<5)$. $B=a_0+a_1x+a_2x^2+a_3x^3$, $X_{A_1}/R_0=b_0+b_1x+b_2x^2$ $(x=X_{A_1}/X_{A_2})$.

A_1	A_2	a_0	a_1	a_2	a_3	b_0	b_1	b_2
14	12	−2236.76	2604.77	0	0	0.794 846	−0.732 872	0
12	10	−1364.42	1632.34	0	0	0.853 417	−0.784 096	0
10	8	−756.083	939.847	0	0	0.940 158	−0.862 697	0
8	6	−363.763	479.243	0	0	1.080 41	−0.996 187	0
6	4	584.402	−1869.47	1482.2	0	1.337 46	−1.257 79	0
4	3	777.432	−2093.06	1404.85	0	2.069 81	−1.873 76	0
3	2	−16448.1	57496.3	−67 108.9	26151.8	−3.843 18	13.1556	−9.132 74
2.5	2	−7177.12	25260.1	−29 706.2	11672	−1.652 24	8.468 70	−6.524 01
2	1.5	−2512.90	8758.01	−10 214.3	3985.89	0.812 347	2.993 44	−3.306 57
1.5	1.2	−4385.53	14 060.8	−15 059.8	5388.11	−0.118 389	5.922 42	−5.059 29
1.2	1.0	−5866.50	17 984.6	−18 406.7	6289.13	0.974 026	4.597 56	−4.646 48
1.0	0.9	−21833.8	65 663.3	−65 861.6	22031.9	1.41521	7.153 89	−7.528 78
0.9	0.8	−7603.63	23 031.7	−23 264.7	7836.33	−14.3971	−18.7314	5.461 63

curve is usually less than 0.1 pixel (≈ 1 μm). Note that there are many sets (A_1, A_2) which can be used to obtain the values of B and R_0. As mentioned in Sec. I, more accurate B and R_0 can be obtained when points closer to the solid surface are selected.

PERFORMANCE

The present method allows one to measure the dynamic/advancing/receding contact angle and the surface (interfacial) tension simultaneously for sessile drops with/without equatorial diameters. The accuracy of surface tension becomes worse as the contact angle of sessile drop is smaller. The accuracy of the measurement of advancing/receding contact angle was examined by testing the contact angle of pure water drops on the surfaces of paraffin film, PMMA, and cover glass at 25.0±0.1 °C. PMMA and cover glass were purchased from Fisher Scientific Co. Paraffin was obtained from American National Can. The water used in all experiments was purified via a Barnstead NANOpure II water purification system. The output water has a specific conductance less than 0.057 μS/cm. The value of the surface tension of air/water interface is 72.0±0.1 mN/m at 25.0 ±0.1 °C, examined using a video-enhanced pendant drop tensiometry.[16] The humidity inside the air chamber is controlled and dependent on time as follows: The humidity of is kept larger than 95% at the beginning 60 s and then goes down to 65% in about 20 min, so, the volume of the sessile drop decreases with time due to the evaporation of water.

The contact angle and drop volume of pure water on the paraffin film are plotted in Fig. 6. The volume keeps nearly constant at the beginning 60 s and then decreases with time. The humidifier was turned off and the door of the air chamber was open after the sessile drop was created for 60 s. The data in Fig. 6 indicate that the contact angle varies very little for the beginning 60 s and it is equal to the advancing contact angle in the literature. The contact angle is then decreases due to the evaporation of water of sessile drop. Figure 6(a) is replotted in Fig. 6(b) in where the time of the last data point in Fig. 6(a) is set to be zero time $(t^*=t_{\text{last data point}}-t=0)$. The change of volume at large time (i.e., at small t^*) is slow, and the contact angle becomes fairly constant and is close to the receding contact angle. The relaxation of surface tension for five sessile drops of water on paraffin is shown in Fig. 7 and the accuracy is worse than the pendant drop technique.[17]

Figure 8 shows a similar result for the PMMA solid. Both drop volume and contact angle keep nearly constant at the first 60 s, then decreases due to evaporation of water. The change of volume at small t^* is slow, the contact angle is nearly constant and is the receding contact angle. The data in

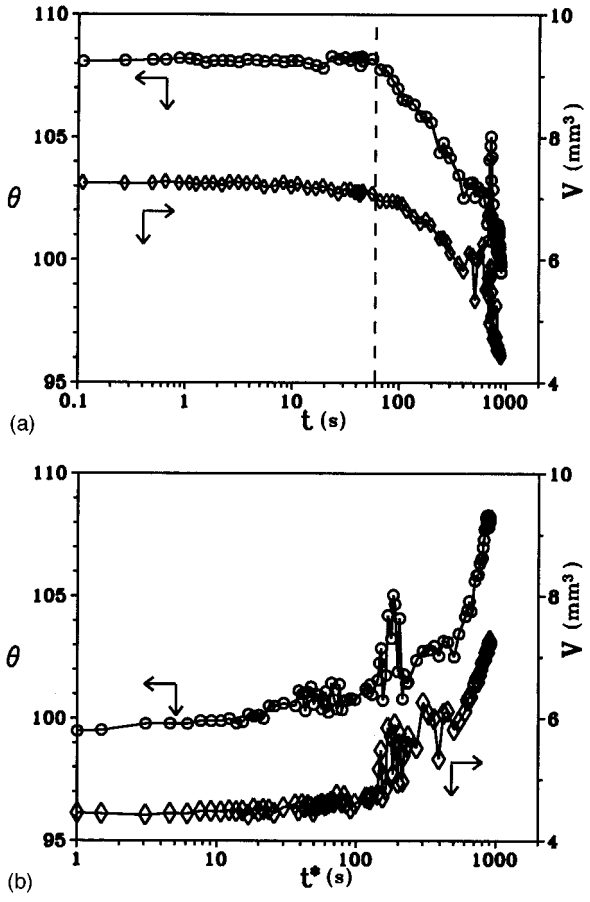

FIG. 6. Experimental values of dynamic contact angle and drop volume for pure water on the paraffin surface plotted as a function of (a) time after drop being created and (b) t^*.

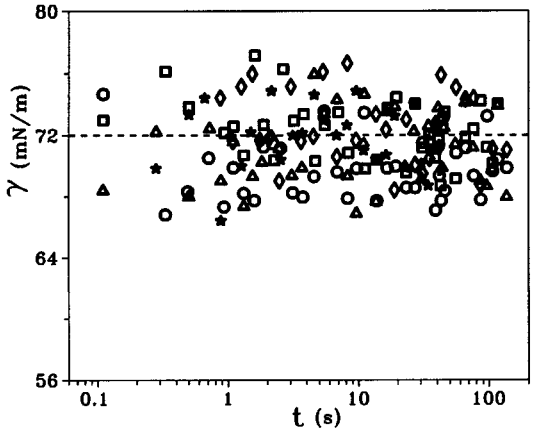

FIG. 7. Experimental values of dynamic surface tension (mN/m) measured from the sessile drop profiles for pure water on the paraffin surface. Each symbol represents a separate sessile drop.

the first 60 s are examined in detail and are replotted in Fig. 9. The variation of volume is less than 0.5% in the first 60 s and this variation is more likely from the error of volume calculation from the best-fit sessile drop profiles. The contact angle keeps at 79.9° for the first 3 s and then decreases slowly for 0.45° for next 60 s. The drop volume at small t^* changes very little, the contact angle at $t^* < 60$ s varies less

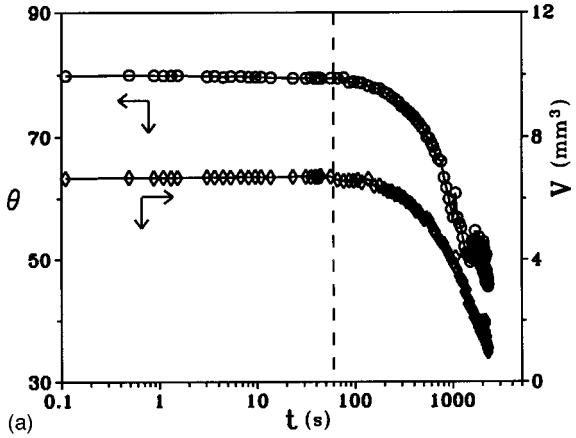

FIG. 8. Experimental values of dynamic contact angle and drop volume for pure water on the PMMA surface plotted as a function of (a) time after drop being created and (b) t^*.

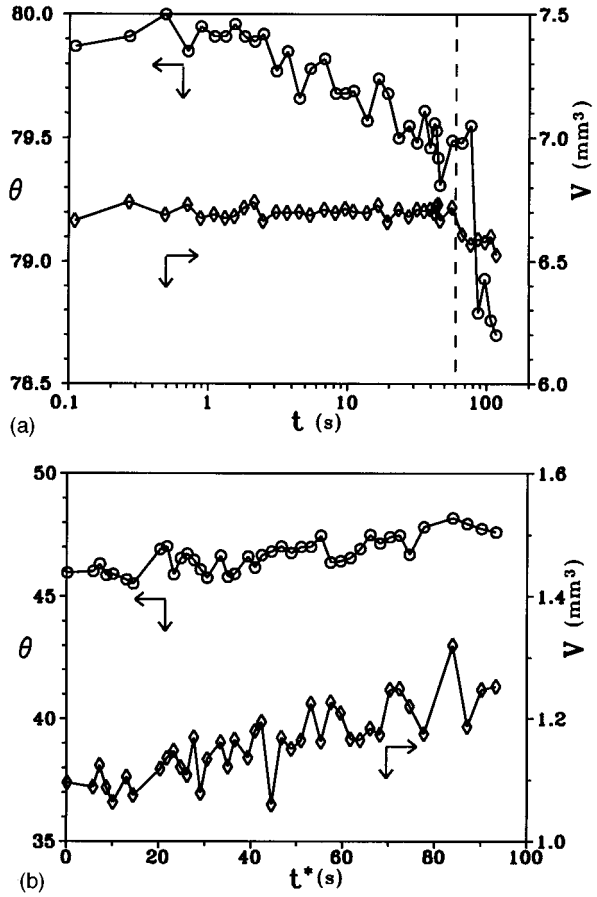

FIG. 9. Dynamic contact angle and drop volume for pure water on the PMMA surface plotted as a function of time at small (a) t and (b) t^*.

than 1°, and the receding contact angle is equal to 46.0°. The three-phase line is a circle for the sessile drop. The diameter of the three-phase contact circle was calculated from the distance of the two contact points of the best-fit drop profile from the drop image and plotted as a function of time in Fig. 10. The diameter of the three-phase contact circle d_s increases slowly for the first 60 s in where the humidity inside the air chamber is around 95%. So, at the first 60 s water

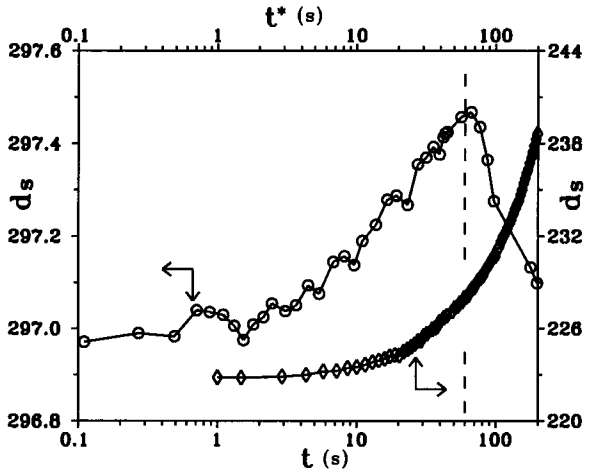

FIG. 10. Experimental values of diameter of the circle of the three-phase line for pure water on the PMMA surface plotted as a function of time at small (a) t and (b) t^*.

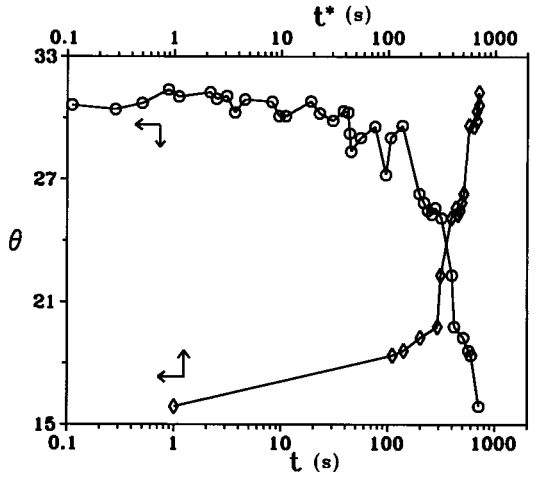

FIG. 11. Experimental values of dynamic contact angle for pure water on cover glass plotted as a function of (a) time after drop being created and (b) t^*.

does advance part of the way across the solid surface and the angle measured is, as defined, the advancing contact angle. A similar analysis was also done for the receding contact angle, shown in Figs. 8(b), 9(b), and 10. At small t^*, the volume of the sessile drop varies little, the contact angle is nearly constant, and the diameter of the three-phase line decreases slowly. Water does recede at this time and the angle measured is the receding contact angle.

The measurement of the contact angle of sessile drop of pure water on the cover glass was done in a similar way. Figure 11 shows the contact angle measured using the present method as a function of time. The humidifier was on for 30 mins and then was turned off; at this time the door of air chamber was open and the cover glass was moved into the chamber and put on the preleveled stage. The sessile drop was then formed in a few seconds. The advancing contact angle is 30.9° and the receding one is around 16°. The variation in this measurement is larger than for paraffin and PMMA. This large variation is likely due to the inhomogeneity of the glass surface since the three-phase line shows as a circle from time to time only, and more often there are several cursor feet around the circle.

The following general conclusions are made about the present system:

(1) This video-enhanced sessile drop tensiometer is an effective tool for the measurement of the dynamic/advancing/receding contact angle; using this feature, we successfully demonstrated the relaxation of contact angle, drop volume, and diameter of the three-phase contact circle;
(2) with this system one is able to monitor the contact angle and surface tension simultaneously;
(3) the contact angles obtained from curve fitting are expected to have greater accuracy than those direct measurements;
(4) this system is suitable for the study of dynamic wetting behavior, such as the behavior of a sessile drop of surfactant solution onto a solid surface or a pure liquid drop onto a solid surface that is soluble into the liquid phase of the droplet.

ACKNOWLEDGMENT

The authors thank the National Science Council, R.O.C., for Grant No. NSC 85-2214-E-011-018.

[1] A. W. Adamson, *Physical Chemistry of Surfaces* (Wiley, New York, 1990), Chap. 10, p. 389.
[2] FACE Contact Angle Meter, model CA-Z, Kyowa Interface Sci. Co., Tokyo, Japan.
[3] Video Contact Angle System, model VCA 2000, Advanced Surface Tech. Inc., MA.
[4] J. B. Cain, D. W. Francis, R. D. Venter, and A. W. Neumann, J. Colloid Interface Sci. **94**, 123 (1983).
[5] R. Y. Tsay, S. C. Yan, and S. Y. Lin, Rev. Sci. Instrum. **66**, 5065 (1995).
[6] Dynamic Contact Angle Analyzer, model DCA-322, CAHN Instruments, Inc., CA.
[7] C. G. L. Furmidge, J. Colloid Sci. **17**, 309 (1962).
[8] E. B. Gutoff and C. E. Kendrick, AIChE J. **28**, 459 (1982).
[9] F. K. Skinner, Y. Rotenberg, and A. W. Neumann, J. Colloid Interface Sci. **130**, 25 (1989).
[10] E. Mooy, P. Cheng, Z. Policova, S. Treppo, D. Kwok, D. R. Mack, P. M. Sherman, and A. W. Neumann, Colloids Surf. **58**, 215 (1991).
[11] C. Huh and R. L. Reed, J. Colloid Interface Sci. **91**, 472 (1983).
[12] Y. Rotenberg, L. Boruvka, and A. W. Neumann, J. Colloid Interface Sci. **93**, 169 (1983).
[13] S. Y. Lin and H. F. Hwang, Langmuir **10**, 4703 (1994).
[14] S. Y. Lin, K. McKeigue, and C. Maldarelli, AIChE J. **36**, 1785 (1990).
[15] B. Carnahan, H. A. Luther, and J. O. Wilkes, *Applied Numerical Methods* (Wiley, New York, 1969).
[16] S. Y. Lin, T. L. Lu, and W. B. Huang, Langmuir **11**, 555 (1995).
[17] S. Y. Lin, L. J. Chen, J. W. Xyu, and W. J. Wang, Langmuir **11**, 4159 (1995).
[18] C. A. Smith and A. B. Corripio, *Principles and Practice of Automatic Process Control* (Wiley, New York, 1985), Chap. 5, p. 165.